LAWRENCE
LIVERMORE
NATIONAL
LABORATORY

UCRL-JRNL-226350

# Conductivity of carbon nanotube polymer composites

J. T. Wescott, P. Kung, A. Maiti

November 27, 2006

Applied Physics Letters

# Conductivity of carbon nanotube polymer composites

James T. Wescott[1]
Accelrys Ltd, 334 Cambridge Science Park, Cambridge, CB4 0WN, UK.

Paul Kung
Accelrys Inc, 10188 Telesis Court, Suite 100, San Diego, CA 92121

Amitesh Maiti[2]
Lawrence Livermore National Laboratory, University of California, Livermore, CA 94551.

[1]E-mail: jwescott@accelrys.com, [2]E-mail: maiti2@llnl.gov

Dissipative Particle Dynamics (DPD) simulations were used to investigate methods of controlling the assembly of percolating networks of carbon nanotubes (CNTs) in thin films of block copolymer melts. For suitably chosen polymers the CNTs were found to spontaneously self-assemble into topologically interesting patterns. The mesoscale morphology was projected onto a finite-element grid and the electrical conductivity of the films computed. The conductivity displayed non-monotonic behavior as a function of relative polymer fractions in the melt. Results are compared and contrasted with CNT dispersion in small-molecule fluids and mixtures.

Keywords: Conductivity nanotube polymer composites

PACS:

A class of nanomaterials receiving much recent attention is that in which single- and multiwalled CNTs are dispersed within polymeric matrices [1]. Such systems could be potentially useful as structural materials, electromagnetic and heat shields, conducting plastics, sensors, biocatalysts, and in many other applications. The overall properties of a CNT-polymer composite material depend strongly on the uniformity of CNT dispersion within the polymer including, for some applications, the degree of orientational alignment, the efficacy of interfacial bonding between the two systems, and the way in which the physical properties of interest depend on the CNT diameter and chirality. Of specific interest to us are properties like electrical and thermal conductivity, which are several to many orders of magnitude higher for pure CNTs than for typical polymers, and require conducting pathways. Therefore, a significant enhancement of such properties for a CNT-polymer composite is expected when a percolation network of CNTs form between two opposite contacts. The percolation problem of rigid rods and sticks has previously been investigated both analytically [2] and through simulations [3, 4]. An important result from such simulations is that the critical volume fraction (CVF) corresponding to the percolation threshold is inversely proportional to the rod's aspect ratio $a$, implying that for CNTs (with typical $a \sim 10^3$-$10^4$) the CVF should be within a few tenths of a percent. Our aim was to re-visit the above problem by incorporating two more realistic materials features: (1) CNTs are not completely rigid, but possess some bending flexibility, and (2) in a multi-component polymer/fluid environment CNTs can display preferential segregation in one component over others, including a tendency to form bundles with other CNTs. Both these features can potentially affect the CVF and hence lead to interesting behavior in the electrical and thermal conductivity.

In this Letter, we perform a specific set of simulations to explore how topological patterns in a block-copolymer system might be exploited to create controlled linkages of CNTs with potentially lower CVF as compared to a completely random CNT-network. More specifically, block copolymer composition can be controlled to self-assemble a variety of phases: lamellar, bicontinuous, gyroid and discrete micelles [5]. Thus, with appropriate choice of polymers more structured arrangements with improved percolation of CNTs at low fractions might be possible.. Template-controlled assembly of CNTs is a problem relevant not only to nanocomposites, but to other diverse application areas [6]. Self-organization of inorganic nanoparticles in copolymers have been investigated both experimentally [7] and computationally [8, 9] and dispersion of stiff rods, somewhat representative of CNTs, have been investigated in fluids and phase-separating fluid mixtures [10].

Considering the rather large length and time-scales involved we embarked on a mesoscale representation using a Dissipative Particle Dynamics (DPD) approach [11], in which monomers are grouped into single "beads". The preferential segregation of one component into another is governed by an interaction parameter $\Delta a$, which can be related to the Flory-Huggins $\chi$-parameter. The connectedness of a polymeric chain is implemented through a 'bond' term between successive beads, while the bending rigidity of a CNT is incorporated through an angle term with a suitable stiffness constant [12, 13]. For clarity of interpretation, as well as to limit computational requirements the simulations reported here are performed on quasi-two-dimensional simulation slab of size 75x75x4 DPD units containing a total of 67500 beads. With the same physical interpretation as in our previous work, the above cell would approximately correspond to physical dimensions of 61 nm containing roughly one million atoms [14]. More importantly, the coarse-graining in DPD extends the effective time-step by several orders of magnitude over conventional molecular dynamics, and a total simulation time of several microseconds to even a millisecond becomes feasible.

Each CNT and polymer chain is chosen to be of length 13 and 20 beads respectively, in keeping with the requirement that they are larger than the thin dimension of the simulation slab but much smaller than the larger in-plane dimensions. In addition simulations in fluids represented by single beads were carried out for comparison. The idea is to use DPD to compute the equilibrium distribution of various components (CNT, polymer, fluid) in the above computational cell, and then to compute electrical and thermal conductivity using a finite-element modeling (FEM) approach [15] as implemented in the MesoProp software [16]. In such an approach, the bead positions of a DPD morphology are first converted into a concentration gradient. This is numerically mapped onto an FEM grid of homogeneous volume elements, the local properties of which are calculated from the fraction of each component phase and its assigned pure component property value. This approach has largely been applied to the calculation of thermoelastic properties of composites [17], including CNT-reinforced polymers [18]. Electrical conductivity can equally well be evaluated for the composite by solving the Laplace equation:

$$\nabla.\{\sigma(\vec{r}).\nabla\varphi(\vec{r})\} = 0, \qquad (1)$$

where $\sigma(\vec{r})$ and $\varphi(\vec{r})$ are the local conductivity and the local electrostatic potential respectively. MesoProp uses an algorithm in which an electric field is applied in the three main directions to the finite element mesh, and then the electrostatic energy of the composite is minimized with a conjugate gradient method [15].

Use of the FEM model requires a suitable choice of pure component conductivities as input. The disparity in electrical conductivity ($\sigma$) of metallic CNTs and polymer is can be almost 20 orders of magnitude with, $10^6$ $Sm^{-1}$ for CNTs [19] compared to $10^{-13}$ $Sm^{-1}$ for regular insulating polymers [20]. Given that even for a percolating CNT network the electrical conductivity can be somewhat limited by CNT-CNT contact resistance [3, 21, 22], we chose a CNT:polymer conductivity ratio of $10^{10}$. Since the morphology constantly evolves during simulation, a time average of representative configurations over long simulation runs (200000 steps or more) was used to generate the in-plane conductivity of the slab. This averaging is especially important around the CVF of CNTs where the percolation network continuously makes and breaks as a function of time (see Fig. 1 (a and b)). Spikes in these graphs show how the conduction depends strongly on the existence of a continuous pathway, jumping from zero to values of $5x10^6$ S/m whilst a pathway exists.

Before tackling the more complicated case of diblock copolymer, we first investigate CNTs in a pure fluid and a pure polymer. Fig. 1 (c) plots the time averaged conductivity for a fixed CNT loading (0.5 %) as a function of the interaction parameter $\Delta a$. This shows; (1) that for both ideally mixed fluid and polymer cases, where $\Delta a$=0, the CVF for CNT percolation is less than 0.5%; (2) that for all values of $\Delta a$ the conductivity in the fluid system ($C_1$) is higher than that in the polymer ($C_{20}$), underlying a greater propensity for CNTs to phase separate from the polymer – we note that for the ideal mixing case (i.e. $\Delta a$ = 0) the conductivity of the fluid system ($C_1$) is about 60% higher than that of the polymer; and (3) for both the fluid and the polymer system the conductivity drastically falls off at around $\Delta a \sim 10$ indicating breakdown of the percolation network due to bundling of the CNTs.

Next we turn to diblock copolymers of $A_nB_{N-n}$, where $N$ is the polymer length in units of DPD beads (chosen to be 20 for concreteness and computational convenience) and $n$ is an integer between 0 and $N$ (inclusive). To ensure the most distinct pattern formation as a function of $n$, $A$ and $B$ must be highly immiscible. We are also most interested in the case in which the CNTs disperse preferentially into one of the polymers, allocated as the $A$ polymer. With specific interaction parameters consistent with the above physical choices, i.e., $\Delta a_{A\text{-}B} = 20$, $\Delta a_{A\text{-}N} = 0$, $\Delta a_{B\text{-}N} = 10$ (and self-interactions $\Delta a_{A\text{-}A} = \Delta a_{B\text{-}B} = \Delta a_{N\text{-}N} = 0$), DPD simulations were performed for different values of $n$ and different CNT fractions (limited to a few percent). Fig. 2 summarizes the results for a fixed CNT fraction (0.75% by volume) as a function of $n$. The left pane shows a few representative configurations from the simulations, while the right pane plots the electrical conductivity of these structures averaged over the whole trajectory of 200000 steps. The conductivity is expressed as a ratio to the

conductivity computed in a pure *A*-polymer (i.e. $n$=20) for the same CNT fraction and an interesting non-monotonic structure as a function of $n$ results. In the following paragraph we try to provide a physical explanation for such behavior.

For pure polymer *B* ($n$=0) a CNT fraction of 0.75% is below the CVF for percolation (consistent with Fig. 1 for $\Delta a$=20) and the conductivity is low. For low fraction of *A*-polymer ($0 < n \leq 6$), regularly distributed islands of *A*-rich material provide domains across which the CNTs bridge. In such case each *A*-micelle is much smaller than CNT-length and CNTs span several *A*-micelles. The *A*-micelles cover approximately $d/s$ fraction of CNT-length (where $d$ = micelle dimension, $s$ = inter-micellar separation), and the equilibrium morphology consists of bundles of CNTs piercing through several *A*-micelles. Such arrangement would not be expected to be efficient in providing a fully percolated network of CNTs, consistent with low conductivity in this region. With increasing $n$ two important morphology changes take place: (1) several *A*-micelles coalesce into elongated micelles, which remain isolated from each other ($n$=8); and (2) the elongated *A*-micelles merge into a percolating *A*-network ($n \geq 10$). In the first case, the CNTs may or may not form a percolating network depending on whether the CNT-length is greater or less than the elongated (but isolated) micelle-length. In the second case (i.e. $n \geq 10$) the CNTs form a percolating network leading to significant conductivity. For the case where *A* is the minority polymer ($n \leq 10$), Fig. 3 displays conductivity for various CNT loading fractions. One observes that the non-monotonic behavior of conductivity as a function of $n$ persists for CNT loading up to ~ 2%, and at higher loadings the behavior becomes monotonic.

Let us now consider the conductivity values for the case where *A* is the majority polymer ($n \geq 10$). If *A* and *B* were small-molecule fluids rather than polymers, then around a 50-50 *A*-*B* mixture one would expect a predominantly layered morphology with nearly flat (percolating) alternating layers of pure *A* and pure *B*. With all the CNTs residing in the *A*-regions, the formation of a CNT-percolation network would then be decided by the CVF within the pure *A*-phase. Thus for a nearly 50-50 *A*-*B* mixture, one can expect the net CVF of CNT to be lowered by approximately 50%. This implies that there is a range of CNT-loading, which will form a percolating network in the fluid mixture but not in the pure "ideal" fluid A. In addition, the CNTs themselves can significantly influence the fluid morphology, which can further aid in the formation of percolating networks [10]. In contrast, the morphologies resulting from diblock copolymers are somewhat rigid. More specifically, for $n$ = 10 the domains are inter-penetrating, and not straight. Sharp turns and kinks within the pure *A*-domains hinder the formation of CNT networks. Fig. 4 compares the computed conductivity of pure *A* polymer and the

$A_{10}B_{10}$ diblock copolymer as a function of CNT-loading. As can be seen, the CVFs are almost the same for both systems, with slightly greater conductivity for the pure polymer system for all values of CNT-loading. This is consistent with all the conductivities in Fig. 3 being less than 100% of the pure polymer conductivity, except at $n$ = 14 where it is slightly more than 100%. We note that application of shear provides alignment [12, 23] to the $A_{10}B_{10}$ polymer phase leading to parallel A-B lamellae and CNTs completely excluded from the B polymer domains. This increases $\sigma/\sigma_{ideal}$ to a value of around 10 i.e 10 fold more effective conduction than isotropic dispersion in the ideal $A_{20}$ polymer. Conduction perpendicular to the layers in this case is completely suppressed.

Finally, we note that within the FEM model, the calculation of thermal conductivity is completely equivalent to that used for electrical conductivity, with $\sigma(\vec{r})$ and $\varphi(\vec{r})$ in eq. (1) replaced by the local thermal conductivity $\lambda(\vec{r})$ and local temperature $T(\vec{r})$ respectively [15]. Again, pure component values need to be assigned. Thermal conductivities for polymers are typically of the order of 0.2 $Wm^{-1}K^{-1}$ e.g. $\lambda$ (PMMA)=0.193$Wm^{-1}K$ [20]. For CNTs however, the range reported is between 30 $Wm^{-1}K^{-1}$ and 6600 $Wm^{-1}K^{-1}$ [24]. The ratio $\lambda$(CNT)/$\lambda$(polymer) is therefore between three to five orders of magnitude, rather than the ten or more orders of magnitude used in our $\sigma$ calculations. Not-too-large $\lambda$-ratio (e.g. ~ $10^3$) coupled with small CNT loading fraction tends to wash away the sharpness in the thermal conductivity enhancement at the onset of CNT-percolation, which could be further suppressed due to enhanced phonon-scattering at the CNT-CNT interfaces.

**Acknowledgement**: We would like to thank Accelrys for the support of this work. The work at LLNL was performed under the auspices of the U.S. Department of Energy by the University of California Lawrence Livermore National Laboratory under Contract W-7405-Eng-48.

**References:**


1. P. M. Ajayan. L. S. Scadler, and P. V. Braun, "Nanocomposite Science and Technology," Wiley-VCH, Weinheim (2003).
2. X. Wang and A. P. Chatterjee, J. Chem. Phys. **118**, 10787 (2003).
3. M. Foygel, R. D. Morris, D. Anez, S. French, and V. L. Sobolev, Phys. Rev. B **71**, 104201 (2005).
4. S. S. Rahatekar , M. Hamm, M. S. P. Shaffer and J. A. Elliott, J. Chem. Phys. **123**, 134702 (2005)
5. E.L. Thomas, D.M. Anderson, C.S.. Henke and D. Hoffman, Nature **334**, 598 (1988); F.S. Bates, M.F. Shultz, A.K Khandpur, S. Forster, J.H. Rosedale, K. Almdal and K. Mortensen, Faraday Discuss **98**, 7 (1994); A.K Kandpur, S. Forster ,F.S. Bates, I. W. Hamley, A.J. Ryan, W. Bras, K. Almdal and K. Mortensen, Macromolecules **28** 8796 (1995); M.F. Shultz, A.K Khandpur, F.S. Bates, K. Almdal, K. Mortensen, D.A. Hajduk and S.M. Gruner, Macromolecules **29** 2857 (1996); M.A. Hillmyer, F.S> Bates, K. Almdal, K. Mortensen, A. J. Ryan and J.P.A. Fairclough, Science **271** 976.
6. Y. Wang, D. Maspoch, S. Zou, G. C. Schatz, R. E. Smalley, and C. A. Mirkin, Proc. Nat. Acad. Sci. **103**, 2026 (2006).
7. Y. Lin et al., Nature **434**, 55 (2005).
8. J. Y. Lee, Z. Shou, and A. Balazs, Phys. Rev. Lett. **91**, 136103 (2003).
9. R. B. Thomson, V. V. Ginzburg, M. W. Matsen, and A. C. Balazs, Science **292**, 2469 (2001).
10. G. Peng, F. Qiu, V. V. Ginzburg, D. Jasnow, and A. C. Balazs, Science **288**, 1802 (2000).
11. R. D Groot and P. B. Warren, J. Chem. Phys. **107**, 4423-4435 (1997).
12. A. Maiti, J. T. Wescott and P.Kung, Mol. Sim. **31**, 143 (2005).
13. A. Maiti, J.T. Wescott, and G. Goldbeck-Wood, Int. J. Nanotechnology **2**, 198 (2005).
14. Based on the assumption that the A bead represents one monomer of PMMA polymer as described in [12].
15. A. A. Gusev, Macromolecules **34**, 3081 (2001).
16. http://www.accelrys.com/products/mstudio/modeling/polymersandsimulations/mesoprop.html .
17. A. A. Gusev and J. J. M. Slot, Adv. Eng. Mater. **3**, 427 (2001); O. A. Goussev, P. Richner, M. G. Rozman and A. A. Gusev, J. Appl. Phys. **88**, 4013 (2000); A. A. Gusev, P. J. Hine and I. M. Ward, Comp. Sci. Techn. **60**, 535 (2000); A. A. Gusev and H. R. Lusti, Adv. Mater. **13**, 1641 (2001); M. Wissler, H. R. Lusti, C. Oberson, A. H. Widmann-Schupak, G. Zappini and A. A. Gusev, Adv. Eng. Mater. **5**, 113 (2002); A. A. Gusev, Phys. Rev. Lett. **93**, 034302 (2004).
18. H. R. Lusti and A. A. Gusev, Modelling Simul. Mater. Sci. Eng. **12**, 101-105 (2004).
19. H. Dai, E.W. Wong and C.M. Lieber, Science 272 523 (1996)

20. Polymer Handbook, 4th Ed. J. Brandrup, E H. Immergut, and E A. Grulke, eds. John Wiley & Sons (2003).

21. Z. Yao, C. L. Kane, and C. Dekker, Phys. Rev. Lett. **84**, 2941 (2000).

22. A. Buldum and J. P. Lu, Phys. Rev. B **63**, 161403 (2001).

23. A. W. Lees and S. F. Edwards, J. Phys. C **5**, 1921 (1972).

24. J. Wang and J-S. Wang, Appl. Phys. Lett. **88**, 111909 (2006), and references therein.

Figure Captions:

Figure 1: (Color Online) (a) and (b) Plots of instantaneous in-plane conductivity in x and y direction versus DPD step number for 0.5 vol% $N_{13}$ rods dispersed in C1 beads and in $C_{20}$ polymer chains respectively (Inset: Typical CNT distributions). The simulation grid was of dimension 75x75x4. Polymer segments are fully flexible, the $N_{13}$ CNT molecules are stiffened through the addition of the bond angle potential reported in [13]. (c) Plot of average conductivity versus interaction strength $\Delta a_{NC}$ for the two cases.

Figure 2: (Color Online) Plot of typical morphologies for 0.75 vol% CNTs in $A_nB_{(20-n)}$ block co-polymers. Polymer density fields shown using white (A material) and back (blue online) (B material). Instantaneous positions of the CNTs beads are shown in grey (red online). Morphologies were generated using $\Delta a_{A-B}$=20, $\Delta a_{N-B}$=10, $\Delta a_{N-A}$=$\Delta a_{N-N}$=$\Delta a_{A-A}$=$\Delta a_{B-B}$=0.

Figure 3: (Color Online) Dependence of the average in-plane electrical conductivity on the $A_nB_{(20-n)}$ diblock copolymer composition and CNT loadings (in vol%). Colouration provides contours at 20%, 40% and 60% levels for $\sigma/\sigma_{ideal}$.

Figure 4: (Color Online) Comparison of percolation threshold for CNT immersed in $A_{10}B_{10}$ diblock and ideal $A_{20}$ polymer only. The onset of conduction is shifted by approximately 0.1 vol%.

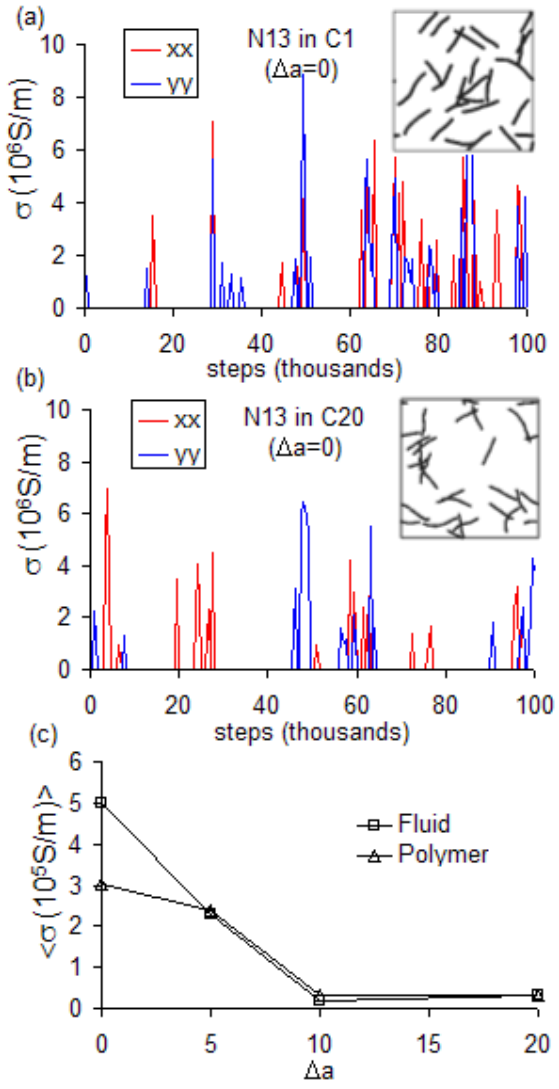
(a)
xx
yy
N13 in C1
(Δa=0)
σ (10⁶S/m)
steps (thousands)
(b)
xx
yy
N13 in C20
(Δa=0)
σ (10⁶S/m)
steps (thousands)
(c)
Fluid
Polymer
<σ (10⁵S/m)>
Δa

Fig. 1

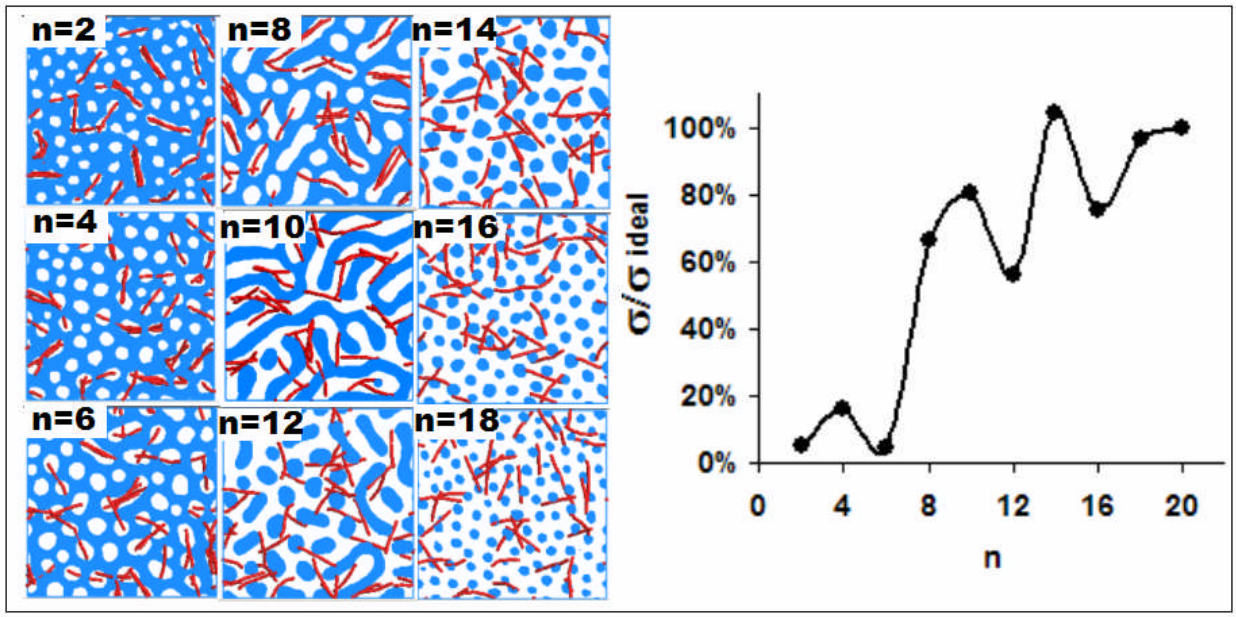
n=2
n=8
n=14
n=4
n=10
n=16
n=6
n=12
n=18
σ/σ ideal
100%
80%
60%
40%
20%
0%
0
4
8
12
16
20
n

Fig. 2

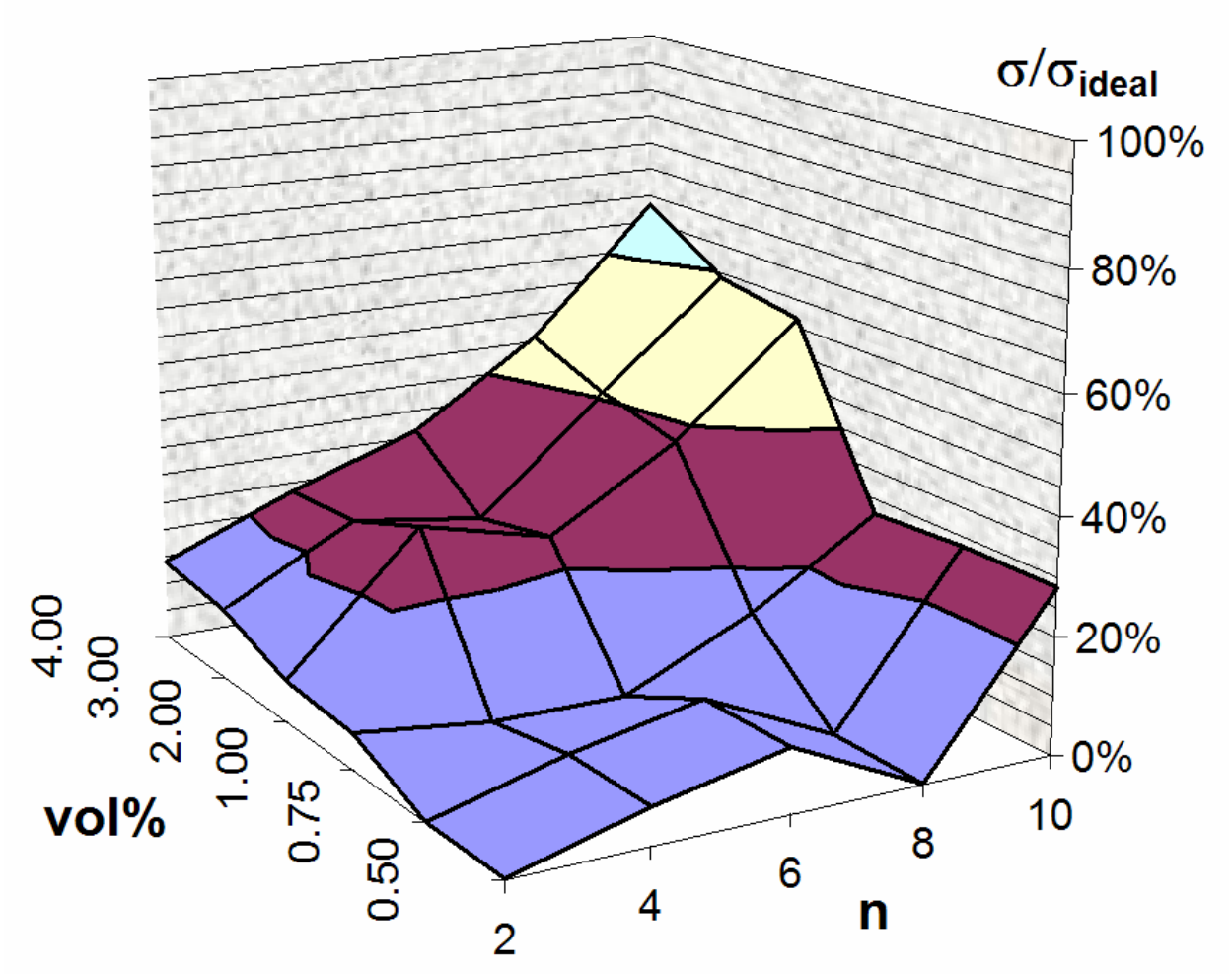


Fig. 3

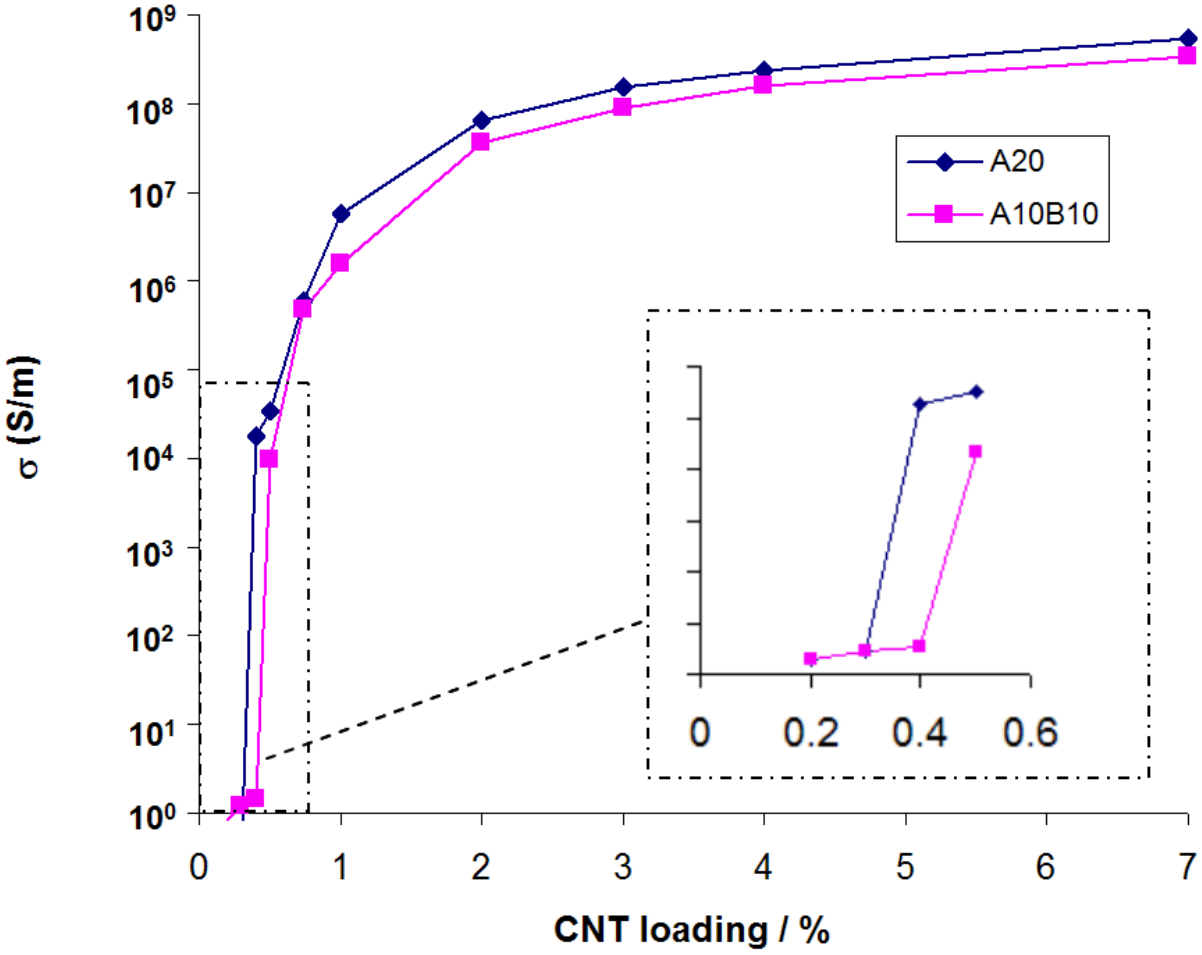
σ (S/m)
10^9
10^8
10^7
10^6
10^5
10^4
10^3
10^2
10^1
10^0
0
1
2
3
4
5
6
7
CNT loading / %
A20
A10B10
0
0.2
0.4
0.6

Fig. 4